Aerodynamics of Ballistic Re-entry Vehicles with Asymmetric Nosetips

D.W. Hall*
General Electric Company, Philadelphia, Pa.
and
D.T. Nowlan†
The Aerospace Corporation, Los Angeles, Calif.

Two numerical techniques for the prediction of inviscid flowfields about re-entry vehicles with asymmetric nosetips are described and validated by comparison to ground test data. One technique is a finite-difference integration of the exact governing equations; the second method presented is an approximate technique suitable for application to statistical dispersion analyses, which retains many features of the more exact approach. The application of such flowfield techniques to the reconstruction of nosetip shapes from flight data is demonstrated.

Nomenclature

C_A = axial force coefficient
C_m = pitching moment coefficient
C_N = normal force coefficient
C_{N_N} = nose normal force coefficient
d_1, d_2 = vertical and horizontal offsets of nose centerline from vehicle axis
h = static enthalpy
H_∞ = freestream total enthalpy
M_∞ = freestream Mach number
p = pressure
q_∞ = freestream dynamic pressure
r = radial coordinate in cylindrical coordinates or radius
$\hat{r}$ = cross-section radius, measured from offset centerline
u,v,w = tangential, normal, and circumferential velocity components in body-normal coordinates
x = axial coordinate
x_{cg} = center of gravity location
x_{cp} = center of pressure location
y = normal coordinate in body-normal coordinates
α = angle of attack
α_T = trim angle of attack
ϵ = damping parameter for iterative solution
θ = surface inclination angle
θ_c = frustum cone angle
ρ = density
τ = w/u
ϕ = circumferential coordinate
ψ = stream function

Subscripts

b = body surface or base quantity
EB = equivalent body quantity
L = lee plane quantity
n = nose quantity
S = side plane quantity
s = shock quantity
W = wind plane quantity
0 = stagnation streamline quantity
α = $\partial/\partial\alpha$

Presented as Paper 77-701 at the AIAA 10th Fluid and Plasmadynamics Conference, Albuquerque, N. Mex., June 27-29, 1977; submitted June 23, 1977; revision received Oct. 28, 1977.

Index categories: Supersonic and Hypersonic Flow; LV/M Aerodynamics; Computational Methods.

*Engineer, Advanced Aerothermodynamics, Re-entry and Environmental Systems Division. Presently, Staff Scientist, Science Applications, Inc., Valley Forge, Pa. Member AIAA.

†Manager, Re-entry Vehicle Technology, Concepts and Plans Directorate. Member AIAA.

Introduction

FOR ballistic re-entry vehicles, one of the primary sources of vehicle dispersion at low altitudes is the roll-trim effect. Dispersion results when lift forces, such as created by a trim angle-of-attack condition caused by the formation of an asymmetric nose shape, are not integrated out by the spin of the vehicle. Prediction of vehicle dispersion is critical to the design and evalutation of accurate re-entry systems.

The characterization of dispersion due to the roll-trim effect requires a coupling of the vehicle's dynamics with its aerodynamic characteristics along the entire entry trajectory. One of the critical features for such an analysis is the prediction of nonrolling trim angles of attack generated through asymmetric ablation of the nosetip. Thus, accurate dispersion modeling requires two fundamental capabilities: the ability to define the time-dependent shape change of the nosetip and, given the nose shape, the ability to evaluate the aerodynamic characteristics of the vehicle. This paper is concerned with the latter of these two problems, i.e., the prediction of the aerodynamics of vehicles with known asymmetric nosetips. Results presented in this paper are a summary of the results reported in Refs. 1-3.

Because of the inherent uncertainties in nose shape change predictions, the prediction of re-entry vehicle dispersion is generally evaluated statistically. Given a nose shape, however, the prediction of aerodynamic characteristics is a deterministic problem. Fortunately, at the flight conditions of interest (and in most hypersonic wind tunnels simulating re-entry conditions at low altitudes), the Reynolds number is sufficiently large that the shock layer is entirely inviscid, except for the small viscous (boundary) layer at the vehicle surface. Additionally, conditions are such that the flow is in the weak viscous-inviscid regime; thus, viscous shear and induced pressure effects will significantly affect only the axial force experienced by the vehicle. Other vehicle forces and moments (normal force and pitching moment) can then be accurately determined solely through consideration of the inviscid pressure distribution.

This paper presents methodologies currently available for the prediction of inviscid aerodynamic characteristics for

ballistic re-entry vehicles, with particular emphasis on their abilities to accurately predict the nonrolling trim angle of attack created by asymmetric nose geometries. (The dynamics of a spinning vehicle will amplify the trim angle experienced by a nonrolling vehicle at simialr conditions.) Such aerodynamic predictions can serve two functions. First, as discussed earlier, the determination of vehicle aerodynamics for a given nose shape is an integral part of any dispersion analysis. Second, this aerodynamic prediction capability can be used in conjunction with recession data obtained in flight to reconstruct possible nose shape histories experienced during re-entry. In such a reconstruction, nose shapes are sought that agree with the limited recession data available (generally no more than three rays) and which exhibit aerodynamic characteristics agreeing with those derived from the vehicle's motion history.

Two methods of analytically predicting the inviscid aerodynamics of ballistic re-entry vehicles are presented, and predictions obtained from both techniques are compared to pertinent ground test data. The first technique is the Three-Dimensional Flowfield (3DFF) code,[4,5] which is a numerical solution of the exact inviscid equations of motion. A complete flowfield approach, this code is not only capable of accurately predicting the flow about asymmetric noses, but it also implicitly models the influence of the asymmetric nose on the afterbody flowfield. This effect will be shown to be an important factor in the accurate prediction of trim characteristics of asymmetric-nosed configurations.

The second technique presented is an approximate flowfield technique, developed to model the important features of three-dimensional flowfields in a fraction of the computer time required by the more rigorous exact technique. This approximate technique, the Three-Dimensional Shock and Pressure (3DSAP) code,[3] is suitable for application to statistical dispersion analysis codes, where the inviscid environment must be evaluated many times along a given trajectory, a task for which complete flowfield techniques would be prohibitively expensive.

Ground test data are used to evaluate both the exact and approximate flowfield techniques. Reference 1 provides a complete bibliography and evaluation of the available ground test data that pertain to ballistic re-entry vehicles with asymmetric nosetips.

Exact Inviscid Flowfield Solutions

Aside from expensive and time-consuming wind-tunnel tests, the most accurate and reliable method for prediction of aerodynamic characteristics is the numerical integration of the inviscid equations of fluid motion. (Such procedures are exact in the sense of integrating the exact governing equations.) One technique for the numerical solution of these equations is the Three-Dimensional Flowfield (3DFF) code, which is a direct method, in that shock shape and shock layer properties are determined automatically for a specified body shape and freestream conditions. Either ideal gas or equilibrium real gas thermodynamics may be used in the calculations. This system consists of two codes: a transonic procedure for the calculation of the subsonic flow region surrounding the stagnation point and a supersonic procedure for the calculation of the supersonic afterbody flow.

The transonic portion of this technique is a finite-difference solution of the time-dependent inviscid equations cast in a spherical coordinate system. Starting from an assumed initial flowfield, the solution is advanced in time until the steady-state solution is approached asymptotically. The governing equations are written in Euler (nonconservation) form, and thus, strong embedded shocks cannot be treated with this technique. This transonic code is an extension of the technique developed by Moretti.[6]

The supersonic afterbody code is a forward marching integration of the steady inviscid flow equations written in a cylindrical coordinate system, with provision for an axis offset from the vehicle centerline. The required initial data for the afterbody solution are obtained by interpolation on the transonic flowfield solution. This afterbody code determines forces and moments at each axial station computed, providing aerodynamic characteristics as functions of bluntness with a single calculation for a given nose shape, angle of attack (and/or yaw), and freestream conditions. Technical details on this flowfield procedure are beyond the scope of this paper but may be found in Refs. 4 and 5.

Comparison of Exact Inviscid Flowfield Solutions to Tunnel Data

The exact technique just described has been extensively validated by comparison to both flight and ground test data for relatively simple vehicle geometries, such as sphere-cones and sphere-biconics (e.g., Refs. 4 and 5). Results presented in this paper will concentrate on the capability of this code relative to the low-altitude dispersion problem of aerodynamic evaluation of re-entry vehicles with ablated nose shapes. Because of the uncertainty that exists in the determination of ablating nose shapes that occur in flight, the predictions will be compared to ground test data, where the actual nose shape and ambient flow conditions are accurately known. Since the total temperature in hypersonic wind tunnels is low enough that real gas effects on the flowfield are small, ideal gas thermodynamics were used for the calculations presented subsequently, assuming a constant isentropic exponent of 1.4.

For axisymmetric nose shape comparisons, predictions were made at one angle of attack (typically 0.5 deg). Since the pitching moment and normal force coefficients are known to vanish at $\alpha = 0$ for axisymmetric shapes, values of C_{m_α} and C_{N_α} at $\alpha = 0$ deg are determined by assuming linear aerodynamics (constant C_{m_α}, C_{N_α}) over the small angle-of-attack range $0 < \alpha < 0.5$ deg. The validity of this assumption is verified by comparison of predictions to tunnel data for the axisymmetric shapes presented later. (Accurate aerodynamic predictions have been made with this exact technique for angles of attack as high as $\alpha/\theta_c \approx 3$. Such conditions are more typical of maneuvering than of ballistic re-entry vehicles and hence, comparisons of predictions to data at these high angles of attack are beyond the scope of this paper.)

The predictions are compared to tunnel data for axisymmetric shapes in Figs. 1 and 2. Figure 1 demonstrates the capability of this flowfield technique to accurately predict normal force and pitching moment coefficients at a Mach number of 5 for an ablated shape that might result from laminar flow on a carbonaceous nose.

As the boundary layer on the nose passes through transition to a fully turbulent state, the character of the nose shape changes, such as illustrated by the turbulent nose shape shown in Fig. 2. (Actual nose shapes experienced in flight are complex functions of trajectory, environment, erosion, etc.) Also shown in this figure are tunnel data obtained on this axisymmetric shape at $M_\infty = 5$ and the corresponding numerical predictions. The predictions are seen to be in ex-

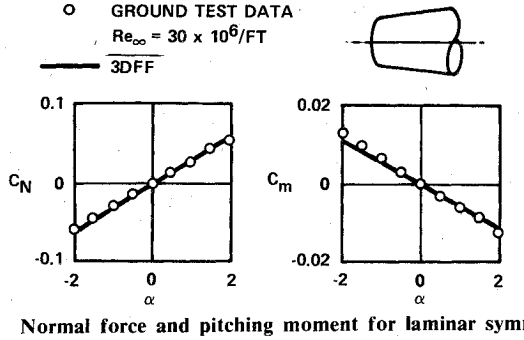

Fig. 1 Normal force and pitching moment for laminar symmetric shape at $M_\infty = 5$.

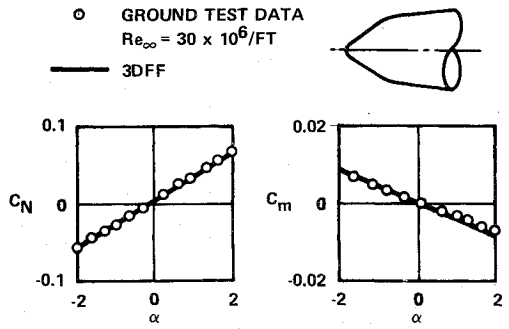

Fig. 2 Normal force and pitching moment for turbulent symmetric shape at $M_\infty = 5$.

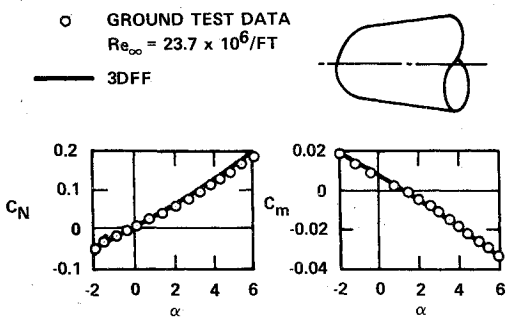

Fig. 3 Normal force and pitching moment for laminar asymmetric shape at $M_\infty = 5$ (exact technique).

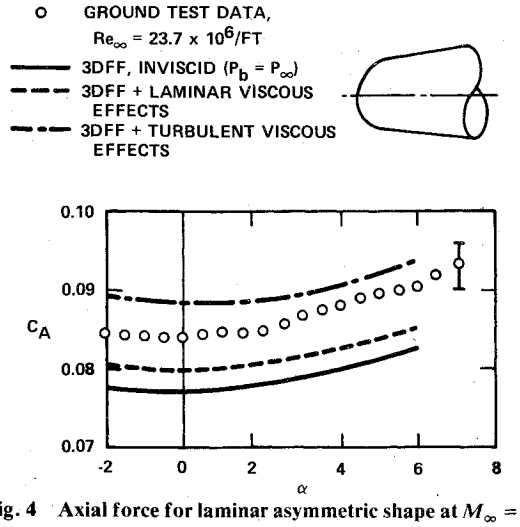

Fig. 4 Axial force for laminar asymmetric shape at $M_\infty = 5$.

cellent agreement with the ground test data for this configuration.

Axisymmetric shapes, however, are not of direct interest in the investigation of the nose trim effect, since nonzero trim angles of attack occur only for nonsymmetric vehicle geometries (assuming that the center of gravity is not offset from the vehicle centerline), such as result from asymmetric ablation on the nose. Unlike the axisymmetric shapes, asymmetric shapes require more than one calculation. For the comparisons shown later, calculations were performed at a minimum of two angles of attack, bounding the trim angle determined from the experimental data. The trim angle is determined by interpolation, assuming linear aerodynamics over this small angle-of-attack range. If vehicle aerodynamic characteristics must be determined over a large angle-of-attack range, a sufficient number of calculations must be made to insure an accurate modeling of the nonlinearities of the aerodynamic coefficients.

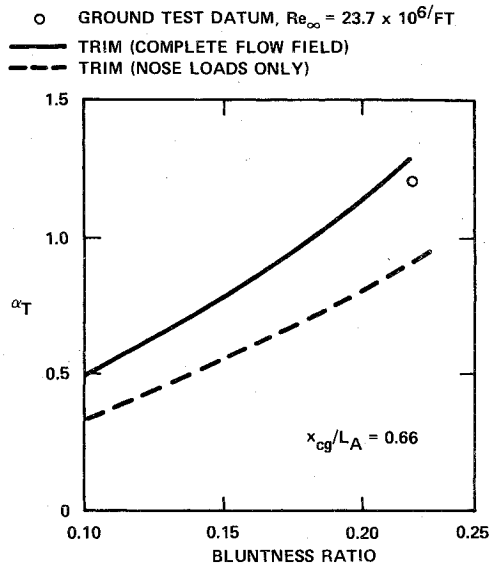

Fig. 5 Trim angle of attack for laminar asymmetric shape at $M_\infty = 5$.

Figures 3 and 4 depict the results obtained from calculations for a typical laminar asymmetric shape at $M_\infty = 5$. Linear interpolation on the C_m predictions predicts a trim angle of 1.28 deg, agreeing quite well with the measured value of $\alpha_T = 1.20$ deg, as shown in Fig. 3. This figure also illustrates the nonlinear behavior of C_m and C_N that can be expected at larger angles of attack.

In Fig. 4, predictions of axial force coefficient are compared to the experimentally determined values for this laminar asymmetric shape. Unlike the pitching moment and normal force coefficients, it is apparent from this figure that accurate prediction of C_A requires consideration of viscous effects, including the state of the boundary layer (i.e., laminar, transitional, or turbulent) along the entire vehicle. The viscous predictons shown in Fig. 4 were obtained from a numerical integration of the three-dimensional integral boundary-layer equations.

Not immediately apparent from the preceding comparisons is the importance of using a complete flowfield technique (i.e., coupled nose and afterbody calculations) for aerodynamic predictions for re-entry vehicles with ablated nosetips. The formation of an asymmetric nose geometry may significantly distort the frustum flowfield, requiring that an accurate afterbody calculation use appropriate initial data obtained from the flowfield prediction for the nosetip. The perturbation on the frustum pressure distribution induced by an asymmetric nose has an important effect on vehicle aerodynamic characteristics, the neglect of which can lead to erroneous predictions of trim angle of attack.

Figure 5 illustrates the hazards of neglecting nose influences on the frustum flowfield. Shown are predicted values of α_T as a function of vehicle bluntness ratio for the laminar asymmetric nose shown in Fig. 3. Also shown in this figure are α_T values predicted using only nose normal force, where α_T is computed from a simple moment balance:

$$C_{N_N}(x_{cg} - x_{cp_{\text{nose}}}) = \alpha_T (C_{N_\alpha})_{sc} (x_{cp_{sc}} - x_{cg}) (r_b/r_n)^2 \quad (1)$$

In the preceding formula, $(C_{N_\alpha})_{sc}$ and $(x_{cp})_{sc}$ are values of these parameters corresponding to an unablated spherically blunted configuration of equivalent bluntness ratio. This moment balance concept is frequently invoked to provide estimates of α_T for an asymmetric nose shape using values of C_{N_N} obtained from Newtonian (or other approximate) surface pressure distributions. The neglect of the influence of the nose shape on the frustum surface pressure distribution inherent in this simple moment balance approach may ad-

versely affect predictions of α_T, as illustrated in Fig. 5. (The value of C_{N_N} used to generate the results shown in Fig. 5 was obtained from the transonic portion of the exact technique.)

Approximate Inviscid Flowfield Solutions

From numerous comparisons of predictions to data, such as previously illustrated, the exact technique has been found to be an accurate, reliable procedure for the prediction of inviscid aerodynamic characteristics of re-entry vehicles with asymmetric nosetips. The efficiency of this exact technique allows its routine use in both design and postflight evaluation efforts. But for some applications, it can require a prohibitive amount of computer time per solution. For example, in a statistical dispersion code, the aerodynamic characteristics of a re-entry vehicle must be determined at many points along a given trajectory. To obtain dispersion statistics, each vehicle must be analyzed many times, each time allowing statistical variation of pertinent parameters (e.g., transition progression, roll torques, etc.). Thus, a large number of aerodynamic predictions can be required to obtain a meaningful prediction of dispersion statistics for a single vehicle along one nominal trajectory.

Use of exact techniques is not consistent with the formulations required in such dispersion models. For this application, an approximate flowfield technique has been developed which requires minimal computer time per solution, while retaining the features of the exact analysis that are critical to obtaining accurate inviscid aerodynamic predictions for vehicles with asymmetric nosetips. This technique is the Three-Dimensional Shock and Pressure (3DSAP) procedure, which, although approximate, is a complete flowfield technique, predicting not only surface pressures, but the entire inviscid shock layer of the vehicle. This code is an extension to three dimensions of the approximate equivalent body flowfield techniques presented in Refs. 7 and 8.

Because of its ability to determine shock shapes as well as surface pressure distributions, this approximate method can be used not only for inviscid aerodynamic predictions, as required for dispersion analyses, but also to provide the data required for viscous analyses when entropy swallowing is considered. Additionally, since the flow over the entire vehicle is considered, it implicitly treats the effect of asymmetric nose geometries on the frustum pressure distribution—an effect important for accurate trim angle-of-attack predicitons, as demonstrated with the results of exact calculations presented earlier.

The nose geometry is specified by defining cross sections of the form $\hat{r}(x,\phi)$ relative to the locus of the cross-section centers, defined from tabulated values of $d_1(x)$ and $d_2(x)$, as illustrated in Fig. 6. The cross sections may be arbitrary in shape, requiring the specification of tabular data, or may be defined analytically for several special cases (e.g., circular or elliptic cross sections). For the frustum, assumed to be axisymmetric, the geometry is defined as shown in Fig. 6.

The calculations in this approximate flowfield technique are performed in a body-normal coordinate system. Body-normal coordinates are ideally suited for use in this technique, since the frustum is axisymmetric and meridional planes on the nose are treated as equivalent axisymmetric bodies; the coordinate surfaces are then closely aligned with the body surface. Calculations may be made using either ideal or equilibrium real gas thermodynamics, using the same gas properties as in the exact technique. Complete details of the analysis may be found in Ref. 3, and are outlined in the following.

On the asymmetric nose, calculations are performed along meridional planes selected by the user. The body surface in each of these meridional planes is treated as an equivalent axisymmetric body; i.e., an axisymmetric body whose axis is parallel to the freestream velocity vector. In the nose region, crossflow is ignored.

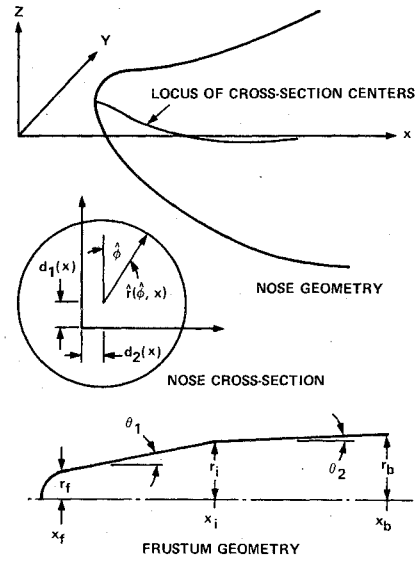

Fig. 6 Geometry definition for approximate flowfield technique.

The nose solution is obtained in two parts: a transonic portion and a supersonic portion. In the transonic region, which runs from the stagnation point to just beyond the sonic point, the surface pressures are assigned from a correlation, and the shock shape is determined iteratively. The transonic portion of the nose flowfield is formulated in vonMises coordinates, where the independent variables are the wetted length and the stream function.

Several assumptions are invoked in the approximate transonic analysis to allow quick calculation of this region of the nose flowfield. (In the exact technique, most of the computer time required per solution for an asymmetric nose case is expended in the transonic region, where the hyperbolic time-dependent equations are integrated in order to avoid the ellipticity of the steady flow equations.)

The first step in obtaining the transonic solution in any meridional plane is the assignment of surface pressures from a correlation. The correlation used is a modification of Love's "Newtonian Deficiency Method"[9] as reported in Ref. 7. An initial estimate of the shock shape in a meridional plane is made using assumed values of standoff distance and a correlation of shock slope vs local body angle.[10]

Properties downstream of the shock are computed as a function of shock slope using the Rankine-Hugoniot conditions. In subsequent iterations on shock shape, the local shock slopes are first determined using a parabolic curve-fitting procedure. Since this procedure uses both upstream and downstream shock locations in the determination of local shock slopes, this approximate transonic procedure retains an "elliptic" character.

Knowing the surface pressures, shock location, and properties downstream of the shock, the flow properties throughout the shock layer can now be determined. It is convenient to divide each body normal being considered into a specified number of segments equally spaced in the stream function, where $\psi = 0$ corresponds to the body surface.

The assumption is made that the pressure profile through the shock layer be expressed as

$$p(\psi) = p_b + (\psi/\psi_s)^2 (p_s - p_b) \tag{2}$$

At the body, where the normal velocity component vanishes, the tangential velocity may be evaluated using a form of the energy conservation relation

$$u = \sqrt{2(H_\infty - h)} \tag{3}$$

The body entropy is assigned the stagnation value, since the stagnation streamline wets the body surface. Along the

equivalent body stagnation streamline ($\psi = 0$) a different assumption is required for the pressure profile. Taking the pressure profile to be parabolic in y,

$$p_0(y) = (p_s - p_b)(y/y_s)^2 + p_b \tag{4}$$

Evaluating the enthalpy along the stagnation streamline from the assumed pressure distribution and the normal shock value of entropy which applies at all points on this streamline, the velocity distribution is

$$v_0(y) = -\sqrt{2(H_\infty - h)} \tag{5}$$

To determine the normal component of velocity throughout the transonic field, a function f_v is constructed based upon the velocity distribution along the stagnation streamline:

$$f_v(y/y_s) = v_0(y)/v_0(y_s) \tag{6}$$

This function is used along all normals (other than the stagnation streamline) to construct the profile of normal velocity as

$$v(\psi) = f_v(\psi/\psi_s)\, v(\psi_s) \tag{7}$$

where $v(\psi_s)$ is known from the calculation of flow properties downstream of the shock.

At each point along a normal (equally spaced in ψ), the value of the stream function is known. Since entropy is conserved along streamlines, the entropy at each point is then known because of the one-to-one relationship between entropy and stream function at shock points in a given meridional plane.

Knowing $s(\psi)$ and $p(\psi)$ along each normal, the local value of enthalpy may be determined from the thermodynamic equations of state. It is then possible to calculate the remaining unknown (tangential velocity) at each point through the field as

$$u(\psi) = \sqrt{2(H_\infty - h) - v^2} \tag{8}$$

At this point the complete transonic flowfield has been determined for an assumed shock shape, utilizing the various assumptions incorporated into the foregoing analysis. However, the mass flow rate through the shock layer may not be consistent with the assumed shock shape. Accordingly, a new shock shape is obtained by computing a new shock distance along each normal, based on the mass flow in a given meridional plane in the computed flowfield:

$$y_s' = \frac{r_{b_{EB}}}{\cos\theta_{b_{EB}}} \left(\sqrt{1 + \frac{2\cos\theta_{b_{EB}}}{r_{b_{EB}}^2} \int_0^{\psi_s} \frac{d\psi}{\rho u}} - 1 \right) \tag{9}$$

This iterative procedure is continued until the computed flowfield is self-consistent, and is accepted as the approximate solution for that plane. New estimates of y_s at each normal are obtained from

$$y_{s_{(new)}} = y_s + \epsilon(y_s' - y_s) \tag{10}$$

where ϵ is typically between 0.6 and 1.0.

Because of its approximate nature, this transonic procedure is capable of obtaining results for any arbitrary nose shape. However, due to inherent limitations in the surface pressure correlation and the assumptions of flow property profiles across the shock layer, accurate results can not be expected for nose shapes exhibiting separated flow regions, strong embedded shocks, or large crossflow velocities.

Once a converged (consistent) transonic solution is obtained in a given meridional plane, the last ray of the transonic region is transformed back to physical coordinates to serve as initial data for the following supersonic flow region. The supersonic region on the nose is computed by integrating the exact steady supersonic equations, which are identical to the three-dimensional equations integrated on the frustum, except that circumferential flow variations are neglected. After each meridional plane on the nose is computed, forces and moments on the nose are obtained from integration of the surface pressures.

Following the determination of the flowfield in each meridional plane on the nose, the frustum calculation is initiated. The frustum flowfield is computed using the same numerical procedure as in the supersonic portion of the exact technique, except that the equations are written in a body-normal coordinate system. Initial data for the frustum calculation are obtained by interpolation on the solutions generated on the nose planes. However, since the frustum calculation explicitly treats crossflow, which was neglected in the nose solutions, an approximate initial distribution crossflow is generated based on the circumferential pressure distribution at the start of the frustum.

To keep the computer time required per solution to a minimum, only four planes are computed on the frustum (three in the case of a pitch plane of symmetry), corresponding to the wind, lee, and two side planes. To retain accuracy with this coarse circumferential spacing, it is necessary to evaluate some circumferential derivatives not by finite differences, but by analytic expressions. In particular, the pressure variation is expressed in each frustum half-plane as

$$p(\phi) = \tfrac{1}{4}(p_L + 2p_S + p_W) + \tfrac{1}{2}(p_L - p_W)\cos\phi + \tfrac{1}{4}(p_L - 2p_S + p_W)\cos 2\phi \tag{11}$$

and the crossflow in each half-plane

$$\tau(\phi) = \tau_S \sin\phi \tag{12}$$

Derivatives are evaluated analytically from Eqs. (11) and (12). These approximations for pressure and crossflow derivatives are very accurate for axisymmetric bodies at small angle of attack; as the angle of attack is increased, however, the approximation to crossflow becomes less accurate as the maximum crossflow velocity magnitude moves off the side plane towards the lee plane. (Good results have been obtained with this procedure for angles of attack as high as $\alpha/\theta_c \approx 1$.) Forces and moments on the frustum are obtained by numerical integration, using Eq. (11) to describe the circumferential pressure distribution.

This procedure retains the features of the exact analysis that are critical to accurate predictions of the frustum pressure distribution, while minimizing the amount of computer time required per solution. As an example, for a typical re-entry vehicle configuration with an asymmetric nosetip, a solution using this approximate technique required 5% of the computer time required by the exact code. Because of its efficiency and accuracy, which will be demonstrated in the following section, this approximate procedure can be applied not only to dispersion analyses, but also to preliminary design and postflight evaluation efforts in a cost-effective manner.

The approximate flowfield technique has been validated by comparison to both ground test data and to predictions obtained from the exact flowfield technique. All results presented in this section were obtained using ideal gas thermodynamics.

Figure 7 illustrates the capability of the technique to accurately determine the aerodynamics of sphere-cone configurations at $M_\infty = 5$ over a 5-deg angle-of-attack range. The predicted values of C_N and x_{cp}/L for three different bluntness ratios for a 9-deg sphere-cone are seen to agree favorably with the predictions obtained with the exact procedure.

The ability to successfully predict sphere-cone aerodynamics is not, of course, the critical test for a technique that is to be applied to the nose-trim problem. Of primary

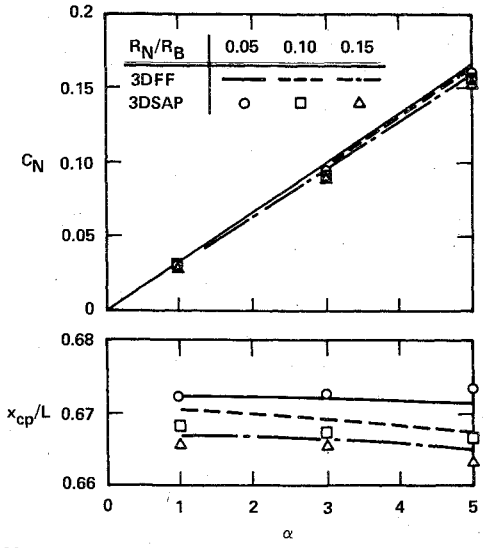

Fig. 7 Normal force and pitch center of pressure for a 9-deg sphere-cone at $M_\infty = 5$.

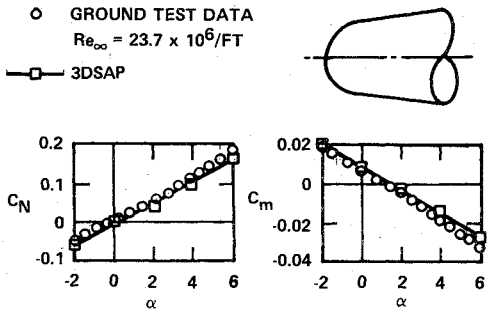

Fig. 8 Normal force and pitching moment for laminar asymmetric shape at $M_\infty = 5$ (approximate technique).

importance to the nose-trim problem is the ability of the approximate technique to predict the aerodynamics of re-entry vehicles with asymmetric nose geometries as shown in the next figure.

Figure 8 depicts the C_m and C_N predictions for the laminar asymmetric shape shown in Fig. 3, compared to ground test data at $M_\infty = 5$ over a wide angle-of-attack range ($-2 < \alpha < 6$ deg). As is to be expected from the assumptions made in the approximate analysis, the accuracy of this flowfield technique is seen to decrease as the magnitude of the angle of attack increases. Assuming linear aerodynamics between $\alpha = 0$ and 2 deg, this approximate technique predicts a trim angle of attack of 1.41 deg for this shape, compared to the values of 1.20 deg (data) and 1.28 deg (exact technique), as presented earlier.

Flight Data Interpretation

The ability to predict the performance of vehicles during re-entry through the atmosphere is the reason for the development of three-dimensional flowfield technology. The aspect of predicting aerodynamic characteristics for known nosetip shapes has been addressed in the foregoing sections. Another important use of this technology is in the analysis of flight test data to infer the character of nosetip shaping necessary to produce the observed motion. No ground test of nosetip ablation can simultaneously generate the instantaneous or time variation of all the governing parameters that occur during re-entry. Only pieces of the problem such as material roughness growth, ablation rates, and flow transition parameters, can be identified on the ground. These data require interpretation and extrapolation by ablation/shape change computational methods to predict nosetip flight

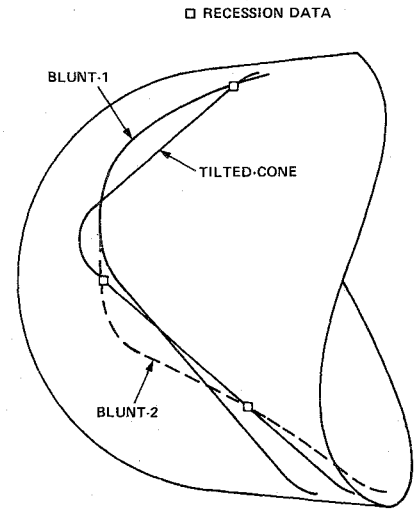

Fig. 9 Postulated asymmetric nosetip shapes.

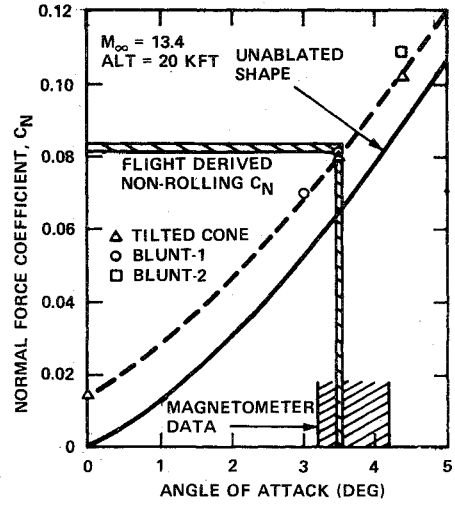

Fig. 10 Normal force coefficient variation for asymmetric nose shapes.

performance. Detailed flight information must be obtained to guide and validate these techniques.

Re-entry vehicle flight test data consist, in general, of measurements of acceleration and angular rate components plus limited nosetip recession measurements (typically, one to three discrete rays of recession sensors). From the dynamics information, the forces and moments acting on the vehicle, the center of force (a stability parameter), and the angle of attack can be computed. At altitudes below 50,000 ft initially symmetric re-entry vehicles develop trim angles of attack which orient into the plane of the wind vector. The asymmetry necessary to accomplish this is attributed to nosetip shaping produced by the asymmetric progression of turbulent flow onto the nose itself. The appearance of this event, combined with the recession sensor measurements, is used by the thermodynamicist to guide analysis of nosetip shaping events. Typically, analyses are made of symmetric nosetip recession with estimates of the degree of asymmetry necessary to produce the observed lateral (lift) accelerations.

Three-dimensional flowfield analyses allow the opportunity to treat all of the re-entry vehicle data as a set during this low-altitude nosetip shaping regime. Guided by thermodynamics and the meridian of the asymmetry, families of shapes can be fit to the recession measurements as a function of altitude. The number of shapes can be reduced by the requirement that the flowfield produced in combination with the vehicle afterbody match the observed trim angle of attack, lateral

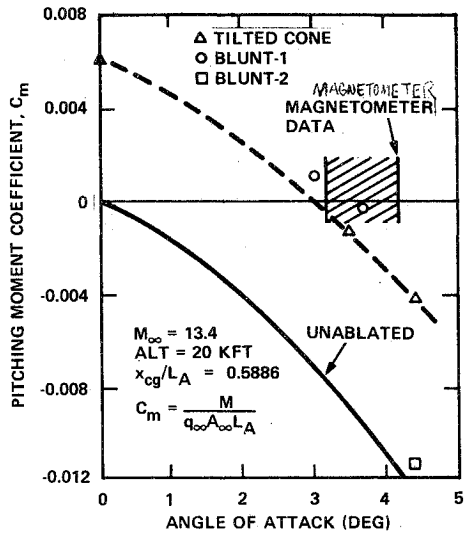

Fig. 11 Pitching moment coefficient variation for asymmetric nose shapes.

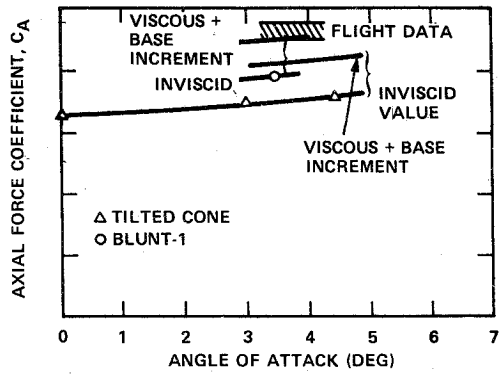

Fig. 12 Axial force coefficient variation for asymmetric nose shapes.

acceleration, axial acceleration, and stability parameters. This process can be continued through re-entry with the additional constraint that the shape change history be thermodynamically consistent.

As an example, consider a single altitude during the re-entry of an initially hemispherically blunted slender cone. In this case, the plane of the trim angle of attack is coincident with the plane of the recession instrumentation. Three postulated shapes, a tilted cone and two blunted asymmetric, that reasonably match the recession data are shown in Fig. 9. In Fig. 10, the predicted normal force coefficient (C_N) variation with angle of attack for each shape and the unablated body are presented. The measured values of C_N and α are shown for reference. From this information nonlinear aerodynamic effects are clearly important for the angle of attack observed on this flight, and the three nosetip shapes considered will all produce the measured normal force, if at the flight angle of attack.

When the pitching moment about the center of gravity is calculated (Fig. 11), only the tilted cone and the blunt No. 1 asymmetric shape produce trim at the correct angle of attack. Since it has been observed that development of an asymmetric nose shape has only a small effect on the shape of the $C_m(\alpha)$ curve [i.e., $C_{m_\alpha}(\alpha)$ is fairly invariant with nose shape], the single calculation for the blunt No. 2 asymmetric shape is sufficient to eliminate this shape from further consideration. When comparing the vehicle axial force created with these two shapes to flight data with increments for viscous and base forces included, it is the blunt asymmetric shape 1 that yields better agreement (Fig. 12).

Conclusions

The techniques presented in this paper represent a significant capability for the analysis of aerodynamic characteristics of ballistic re-entry vehicles with asymmetric nosetips. The exact technique is capable of producing accurate predictions of inviscid vehicle aerodynamics and has found application in both pre- and postflight evaluations. In conjunction with wind-tunnel programs, this code has been used to augment ground test data and to direct support of the design of re-entry vehicles. Used as a postflight tool for nose shape reconstruction, it has provided guidance to the development of shape change models to produce shapes consistent with the observed vehicle motion history. This additional information could be useful to thermodynamicists (i.e., in addition to the recession data) to guide in the reconstruction of the germane parameters required for nosetip shape modeling. For statistical predictions of vehicle dispersion, an approximate flowfield technique has been developed to allow efficient, yet accurate, aerodynamic predictions, critical to obtaining meaningful dispersion estimates. These two techniques provide the aerodynamic prediction capability required to allow the design of optimum ballistic re-entry vehicles in which dispersion has been minimized.

Acknowledgment

This work was supported by Air Force Contract No. F04701-75-C-0152, Subtask 3.1.2.1—Data Analysis.

References

[1] Truncellito, N.T. and Komito, E.H., "Nose Trim Study, Volume I. A Survey and Evaluation of Aerodynamic Ground Test Data on Ablated Nosetip Configurations," Space and Missile Systems Organization (SAMSO) TR-77-46, Sept. 1976.

[2] Hall, D.W., Kyriss, C.L., and Truncellito, N.T., "Nose Trim Study, Volume II. An Evaluation of the G.E. Three-Dimensional Flow Field Program for Ballistic Re-Entry Vehicles with Asymmetric Noses," SAMSO TR-77-46, Sept. 1976.

[3] Hall, D.W. and Kyriss, C.L., "Nose Trim Study, Volume III. An Approximate Three-Dimensional Flow Field Technique for Ballistic Re-Entry Vehicles with Asymmetric Noses," SAMSO TR-77-46, Sept. 1976.

[4] Kyriss, C.L. and Harris, T.B., "A Three-Dimensional Flow Field Computer Program for Maneuvering and Ballistic Re-Entry Vehicles," General Electric Company, Philadelphia, Pa., TIS 75SD013, July 1975.

[5] Hall, D.W., "The Influence of Boundary Point Procedures on Accuracy and Efficiency in Flow Field Calculations," General Electric Company, Philadelphia, Pa., TIS 77SDR016, Mar 1977.

[6] Moretti, G., "Three-Dimensional Inviscid Flow about Supersonic Blunt Cones at Angle of Attack—II. Improved Time-Dependent Techniques for the Blunt Body Problem," General Applied Science Laboratories, Inc., SC-CR-68-3728, Sept. 1968.

[7] Kyriss, C.L. and Neff, R.S., "An Approximate Flow Field Technique for Ablated Re-Entry Eonfigurations," General Eleectric Company, Philadelphia, Pa., TIS 73SD201, Jan. 1973.

[8] Hall, D.W., "An Approximate Technique for the Calculation of Inviscid Hypersonic Flows," General Electric Company, Philadelphia, Pa., TIS 75SDR036, Dec. 1975.

[9] Love, E.S., et al., "Some Topics in Hypersonic Body Shaping," AIAA Paper 69-181, Jan. 1969.

[10] Abbett, M.J. and Davis, J.E., "Interim Report Passive Nosetip Technology Program, Vol. IV, Heat Transfer and Pressure Distribution on Ablated Shapes, Part II, Data Correlation and Analysis," SAMSO TR-74-86, Jan. 1974.